MECSOL 2019 - Proceedings of the 7th International Symposium on Solid Mechanics
V. Tita, A. Ferreira, M.L. Ribeiro, A. Vieira and A.T. Beck (Editors), ABCM, Sao Carlos, SP, Brazil, April 15th to 17th, 2019

An extended Gurson model based approach for constitutive modeling of orthotropic porous solids

Ayrton Ribeiro Ferreira[1,2], Sergio Persival Baroncini Proença[1] and Ahmed Benallal[2]

[1] Department of Structural Engineering, School of Engineering of São Carlos, University of São Paulo, Av. Trabalhador São-carlense, 400, Arnold Schimidt, São Carlos , São Paulo – Brasil, CEP 13566-590
[2] LMT, ENS Paris-Saclay/CNRS/Université Paris-Saclay, 61 Avenue du Président Wilson, Cachan Cedex, F 94235, France

The paper is concerned with the derivation of the effective behavior of anisotropic porous materials, aiming to better represent such materials at failure conditions when subjected to arbitrary stress states. This derivation is based on the acclaimed Gurson model widely recognized as an adequate isotropic framework to model both plasticity and damage evolution for ductile porous materials. The Gurson model is obtained through an upper bound limit analysis on a spherical Representative Volume Element (RVE) with a centered spherical void by prescribing a specific trial velocity field to its domain with such special properties that facilitates the analytical deriving of the effective yield criterion. In this way, the purpose of this work is to extend the Gurson model for porous materials with orthotropic matrix. The orthotropic behaviour of the matrix is an extension of isotropic models taking into account the influence of the second and third stress invariants on the matrix yielding law, following the Hershey-Dalgreen-Hosford (HDH) criterion. All the pores throughout this work are geometrically assumed to be spherical. Therefore, there is no morphological effect on the anisotropy considered here and only the anisotropic yielding of the matrix is considered. Due to the complexity of the new features of this Gurson Model extension, not detailed hereby, the effective yield criterion expressions are presented in a non-closed form. Therefore, for a better understanding of the model response some numerical analyses are then required to illustrate the obtained results. The analyses can be described in two main steps: 1) Firstly, the tensorial direction of the macroscopic strain rate field (E) is varied in the whole range of validity and then the macroscopic stress tensor response for each applied E is computed by using the non-closed expressions of the criterion; 2) In order to properly visualize the yield surface, contour plots of the orthotropic yield surface in planes of interest, as the deviatoric and meridional ones are constructed. The results hereby presented are related to porous materials with different matrix properties, in correspondence to a variation of the HDH coefficients. One concludes about the usefulness of the model as well as its comprehensiveness to include materials with unusual orthotropic parameters.
Keywords: constitutive modeling, ductile fracture, porous media, Gurson model, orthotropy

1 INTRODUCTION

The first works pioneering contributions on ductile failure modeling were given by McClintock (1968) and Rice and Tracey (1969). These authors respectively studied the evolution of porosity in an infinitely elongated hollow cylinder and a spherical void immersed in a sufficiently large matrix. They both concluded that the void growth is highly influenced by the stress triaxiality, which inspired numerous later studies on ductile failure. One among them was Gurson's (1977), who proposed an yield criterion and a damage evolution law for porous ductile materials. Since then, several phenomenological extensions to the Gurson model have been proposed in order to overcome its inherent drawbacks, as the most known works such as Tvergaard (1981), Tvergaard (1982), Tvergaard and Needleman (1984), Koplik and Needleman (1988), Tvergaard (1990) and Nahshon and Hutchinson (2008). Notwithstanding their accurate results for high stress triaxialities, experimental studies pointed out their inefficiency to predict shear dominated failures at low triaxilities (for example, Barsoum and Faleskog (2007) and Nahshon and Hutchinson (2008)). Moreover, despite of their reasonably acceptance for practical purposes, phenomenological approaches still lacks a clear understanding of the theoretical aspects involved in the model. Anisotropy, in terms of complex void shapes but also in the plastic behaviour of the matrix were studied in Gologanu, Leblond and Devaux (1993), Gologanu, Leblond and Devaux (1994), Danas and Ponte Castañeda (2009).

In coherence with the above mentioned aspects, this paper presents an analytical approach to extend the Gurson model for ductile materials whose material matrix exhibits an orthotropic behavior. A general overview of the Gurson (1977) model is firstly introduced. Then, two isotropic analytical extensions including Lode angle effects proposed by Benallal, Desmorat and Fournage (2014) and Benallal (2017) are reviewed. Finally, a mathematical procedure for obtaining the macroscopic yield surfaces for arbitrary orthotropic porous solid is put forward.

2 THE GURSON MODEL

In Gurson (1977), a coupled plasticity and damage model for isotropic ductile materials is proposed. Essentially, a limit analysis upper bound approach is coupled to the Hill-Mandel lemma in homogenization. As shown in Fig. 1, the Representative Volume Element (RVE) is taken as a hollow sphere. Such RVE allows to represent materials whose microscopic defects are randomly distributed without any preferred direction, which therefore configures a macroscopically isotropic behavior. The continuum matrix surrounding the spherical void is assumed to behave as a rigid perfectly-plastic material following a von Mises yield criterion $\phi(\boldsymbol{\sigma}) = \sigma_{eq} - \sigma_0 \leq 0$, where $\sigma_{eq} = \sqrt{\frac{3}{2}\dot{\boldsymbol{\sigma}}' : \dot{\boldsymbol{\sigma}}'}$ and σ_0 is its yield limit stress. Its internal and external radii are defined as a and b, and the porosity $f = \left(\frac{a}{b}\right)^3$ represents the ratio between the spherical volumes of the inner (i.e. void) and outer spheres.

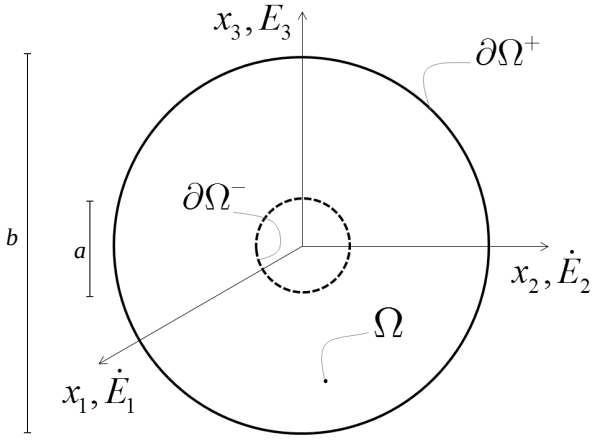

Figure 1: The spherical Representative Volume Element proposed by Gurson (1977).

The internal ($\partial\Omega^-$) and external ($\partial\Omega^+$) surfaces undertake a traction-free ($(\boldsymbol{\Sigma}.\mathbf{n})_{\partial\Omega^-} = 0$) and an uniform macroscopic deformation rate ($\dot{\boldsymbol{\varepsilon}}_{\partial\Omega^+} = \dot{E}$) boundary conditions, respectively, where $\boldsymbol{\Sigma}$ is the macroscopic stress tensor, $\dot{\mathbf{E}}$ is the macroscopic strain tensor and $\mathbf{n}$ is the normal vector of a surface. For convenience both $\boldsymbol{\Sigma}$ and $\dot{\mathbf{E}}$ are splitted in a hydrostatic and a deviatoric parts as showed in Eq. (1).

$$\dot{\mathbf{E}} = \dot{E}_m \mathbf{1} + \dot{E}_{eq}\mathbf{e}' = \dot{E}_{eq}\left(\mathbf{1} + H\mathbf{e}'\right) \tag{1}$$

where $\dot{E}_m = \frac{1}{3}\operatorname{Tr}\dot{\mathbf{E}}$, $\dot{\mathbf{E}}' = \dot{\mathbf{E}} - \dot{E}_m\mathbf{1}$, $\dot{E}_{eq} = \sqrt{\frac{2}{3}\dot{\mathbf{E}}' : \dot{\mathbf{E}}'}$, $H = \frac{\dot{E}_m}{\dot{E}_{eq}}$, $\mathbf{e}' = \begin{bmatrix} \cos\eta & 0 & 0 \\ 0 & \cos\eta - \frac{2\pi}{3} & 0 \\ 0 & 0 & \cos\eta + \frac{2\pi}{3} \end{bmatrix}$ and $\eta = \frac{1}{3}\arccos\frac{4\det\dot{\mathbf{E}}}{\dot{E}_{eq}^3}$.

To obtain the upper bound which defines the effective behaviour, Gurson (1977) uses a trial kinematically admissible velocity field in the kinematic approach of limit analysis. This velocity field $\dot{u}(x)$ is decomposed into two parts, $\dot{u}_G^v$ and $\dot{u}_G^s$, that represent a volume change at a constant shape and a shape change at a constant volume, respectively. $\dot{u}_G^v$ is assumed to be the analytical solution of the RVE under uniform pressure, while $\dot{u}_G^s$ is approximated as $\dot{u}_G^s = \dot{\mathbf{E}}.\mathbf{x}$, for x in Ω. The combination of these two parts gives rise to the Gurson's trial strain rate field tensor in Eq. (2), which respects the kinematic boundary condition in ($\partial\Omega^+$) as well as incompressibility condition.

$$\dot{\boldsymbol{\varepsilon}}_G = \dot{\mathbf{E}}' + \dot{E}_m\left(\frac{b}{r}\right)^3\left[\mathbf{1} + 3\left(\mathbf{e}_r \otimes \mathbf{e}_r\right)\right] \tag{2}$$

where $\mathbf{e}_r$ and r are the versor on the radial direction and the radial coordinate from RVE center, respectively.

Accounting for the upper bound Theorem of Limit Analysis statement, any kinematically admissible field $\dot{u}^*$ other than the exact one, $\dot{u}$, overestimates the energy involved in the failure. Hence, the choice made by Gurson (1977) to the trial velocity field configures an upper bound approach to the RVE mechanical problem. Moreover, in terms of energy, $\pi(\dot{u}_G) >= \pi(\dot{u}^*)$, where π is the microscopic plastic dissipation calculated over the Gurson's RVE. The macroscopic

plastic dissipation potential Π evaluated with $\dot{\boldsymbol{\varepsilon}}_G$ is defined as follows:

$$\Pi(\dot{\mathbf{E}}) = \frac{1}{V}\int_V \pi(\dot{\boldsymbol{\varepsilon}}_G(\dot{\mathbf{E}}))dV = \frac{1}{V}\int_V \sigma_0\sqrt{\frac{2}{3}\dot{\boldsymbol{\varepsilon}}_G : \dot{\boldsymbol{\varepsilon}}_G} = \frac{\sigma_0}{V}\int_V \sqrt{\dot{E}_{eq}^2 - 4\dot{E}_m\left(\frac{b}{r}\right)^3 \dot{\mathbf{E}}' : (\mathbf{e}_r \otimes \mathbf{e}_r) + 4\dot{E}_m^2\left(\frac{b}{r}\right)^6}\, dV \tag{3}$$

where $V = \frac{4}{3}\pi b^3$ is RVE outer sphere volume.

Aiming to simplify the analytical developments, Gurson (1977) argued that a linearization of $\Pi(\dot{u}_G)$ in terms of an auxiliary variable $\mu = \frac{\mathbf{e}_r^T.\dot{\mathbf{E}}_r^T.\mathbf{e}_r}{\dot{E}_{eq}}$ might be made without drastically affecting its accuracy. This linearization makes the product between $\dot{E}_m$ and $\dot{E}_{eq}$ in Eq. (3) disappearing and gives the simplified expression below:

$$\Pi_G(\dot{\mathbf{E}}) = \frac{\sigma_0}{V}\int_V \sqrt{\dot{E}_{eq}^2 + 4\dot{E}_m^2\left(\frac{b}{r}\right)^6}\, dV = \frac{\sigma_0\dot{E}_{eq}}{V}\int_V \sqrt{1 + 4H^2\left(\frac{b}{r}\right)^6}\, dV \tag{4}$$

The macroscopic stresses $\boldsymbol{\Sigma}$ are then derived from $\Pi_G(\dot{u}_G)$ by:

$$\frac{\boldsymbol{\Sigma}}{\sigma_0} = \frac{\partial\Pi}{\partial\dot{\mathbf{E}}} = \frac{2}{3}\ln\frac{2H + \sqrt{f^2 + 4H^2}}{f\left(2H + \sqrt{1+4H^2}\right)}\mathbf{1} + \frac{2}{3}\left(\sqrt{1+4H^2} - \sqrt{f^2+4H^2}\right)\mathbf{e}' = \frac{\Sigma_m^G}{\sigma_0}\mathbf{1} + \frac{\Sigma_{eq}^G}{\sigma_0}\left(\frac{2}{3}\mathbf{e}'\right) \tag{5}$$

where $\Sigma_m = \frac{1}{3}\operatorname{Tr}(\boldsymbol{\Sigma})$ and $\Sigma_{eq} = \sqrt{\frac{3}{2}\boldsymbol{\Sigma}' : \boldsymbol{\Sigma}'}$.

Finally, by combining the expressions to Σ_m^G and Σ_{eq}^G given in Eq. (5) and by eliminating the macroscopic strain rate triaxiality $H = \frac{\dot{E}_m}{\dot{E}_{eq}}$, Gurson (1977) provides his acclaimed yield criterion expression, given by Eq. (6). Figure 2 illustrates both deviatoric and meridional planes of the yield surface obtained by the Gurson model expressions in Eq. (5) and (6) to a material whose initial porosity is $f = 1\%$ and $\sigma_0 = 1$.

$$\left(\frac{\Sigma_{eq}^G}{\sigma_0}\right)^2 + 2f\cosh\left(\frac{3}{2}\frac{\Sigma_m^G}{\sigma_0}\right) - (1+f^2) = 0 \tag{6}$$

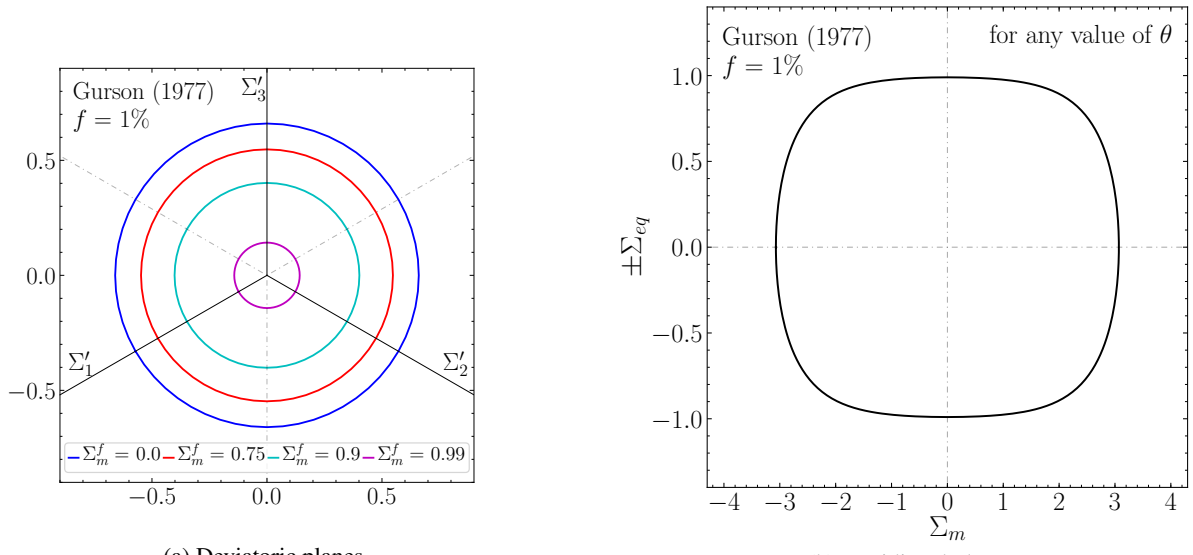

(a) Deviatoric planes

(b) Meridional plane

Figure 2: Yield surface obtained with Gurson (1977) model: (a) deviatoric planes for different levels of $\Sigma_m^f = \Sigma_m/|\Sigma_m^{max}|$ and (b) meridional plane for any macroscopic stress Lode angle θ. The microscopic yield stress is assumed to be unitary for simplicity, $\sigma_0 = 1$.

An important remark is that, even though the macroscopic strain rate tensor is defined by prescribing both its triaxiality H and Lode angle η, the respective macroscopic stress Lode angle is restrained to be equal to η, while its other two mechanical invariants Σ_m and Σ_{eq} depend only on H. This is a direct consequence from the linearization of Π into Π_G.

3 ANALYTICAL ISOTROPIC EXTENSIONS OF THE GURSON MODEL

Benallal, Desmorat and Fournage (2014) assess the role of the linearized microscopic plastic dissipation $\pi_G(\dot{\boldsymbol{\varepsilon}})$ in Gurson (1977) by deriving the macroscopic stress tensor $\boldsymbol{\Sigma}$ directly from the full expression of $\pi(\dot{\boldsymbol{\varepsilon}})$. The complete macroscopic plastic dissipation potential $\Pi(\dot{\mathbf{E}})$ is shown as follows:

$$\Pi(\dot{\mathbf{E}}) = \frac{\sigma_0}{V}\int_V \sqrt{\dot{E}_{eq}^2 - 4\dot{E}_m\left(\frac{b}{r}\right)^3 \dot{\mathbf{E}}' : (\mathbf{e}_r \otimes \mathbf{e}_r) + 4\dot{E}_m^2\left(\frac{b}{r}\right)^6}\, dV = \frac{\sigma_0 \dot{E}_{Eq}}{V}\int_V \sqrt{1 - 4H\mu\left(\frac{b}{r}\right)^3 + 4H^2\left(\frac{b}{r}\right)^6}\, dV \quad (7)$$

The macroscopic stress tensor $\boldsymbol{\Sigma}$ is then obtained by the relation in Eq. (8), in which $\dot{\mathbf{E}}$ is understood as dependent only on the its three mechanical invariants. Due to complexity of the macroscopic plastic dissipation potential in Eq. (7), the resultant yield criterion can no longer be presented by a closed-form expression. Nevertheless, numerical quadratures allow a sufficiently accurate solution to the integral form of $\boldsymbol{\Sigma}$, which permits to evaluate a discrete form of the yield surface.

$$\boldsymbol{\Sigma} = \frac{\partial \Pi}{\partial \dot{\mathbf{E}}} = \frac{\partial \Pi}{\partial \dot{E}_{eq}}\frac{\partial \dot{E}_{eq}}{\partial \dot{\mathbf{E}}} + \frac{\partial \Pi}{\partial \dot{E}_m}\frac{\partial \dot{E}_m}{\partial \dot{\mathbf{E}}} + \frac{\partial \Pi}{\partial \cos 3\eta}\frac{\partial \cos 3\eta}{\partial \dot{\mathbf{E}}} \quad (8)$$

Figure 3 exhibits three yield surface meridional planes correspondent to $\theta = 0$, $\theta = \frac{\pi}{6}$, $\theta = \frac{\pi}{3}$. In order to graphically represent a complete cut plane view of the yield surfaces, negatives values of Σ_{eq} represent the complementary side (macroscopic stress Lode angle $\theta = \bar{\theta} + \pi$) of a half meridional plane ($\theta = \bar{\theta}$). The axisymmetric planes ($\theta = 0$ and $\theta = \frac{\pi}{3}$) slightly deviate from a symmetric plane reference (towards left and right, respectively). As Gurson (1977) had remarked, the linearization of the microscopic plastic dissipation function does not drastically affect the yield criterion for porosities generally involved in ductile fracture ($f \approx 1\%$).

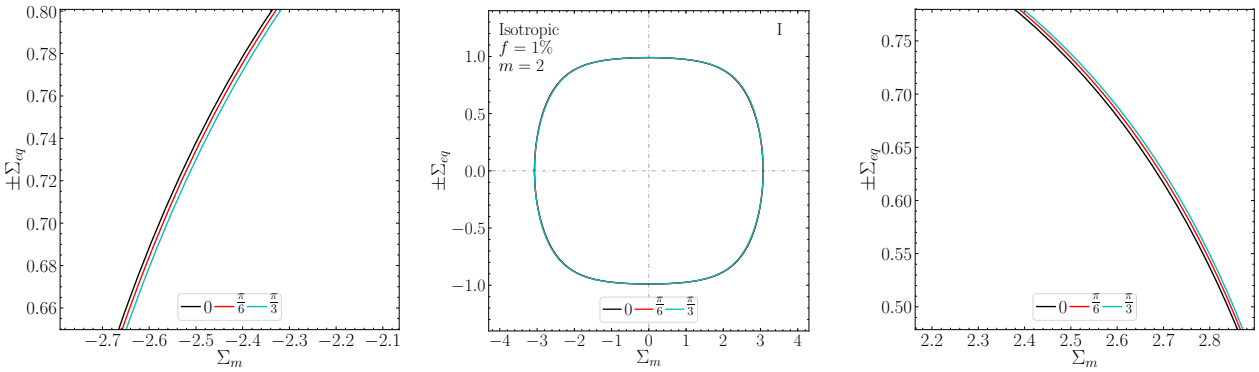

(a) Zoom on the upper left quadrant (b) Meridional planes (c) Zoom on the upper right quadrant

Figure 3: Yield surface for porosity $f = 1\%$ obtained with Benallal, Desmorat and Fournage (2014) model. The microscopic yield stress is assumed to be unitary for simplicity, $\sigma_0 = 1$.

Recently, Benallal (2017) proposes a generalization to the Gurson model for porous materials whose matrix behavior is also dependent on the stress Lode angle besides the von Mises equivalent stress. Essentially, the dependence on the third mechanical invariant of the microscopic stress tensor is analytically inserted in the microscopic yield function $\phi(\boldsymbol{\sigma})$, as shown in Eq. (9). In this way, not only the macroscopic Lode angles η and θ play a role on the yield criterion formulation, but also the microscopic ones ξ and ω, described below.

$$\phi(\boldsymbol{\sigma}) = \sigma_{eq} g(\omega) - \sigma_0 \leq 0 \quad (9)$$

where $\omega = \frac{1}{3}\arccos\left(\frac{27}{2}\frac{\det \boldsymbol{\sigma}'}{\sigma_{eq}^3}\right)$ and $\xi = \frac{1}{3}\arccos\left(\frac{4\det \dot{\boldsymbol{\varepsilon}}_G}{\dot{\varepsilon}_{eq}^3}\right)$.

The function $g(\omega)$ permits to represent different geometrical shapes of the microscopic yield surface on its deviatoric planes, once it is only dependent on the microscopic stress Lode angle ω. This function also must hold the convexity condition, expressed as $g(\omega) + g''(\omega) \geq 0$. Equation (10) shows an example of a function $g(\omega)$ derived from the Hershey-Dalgreen-Hosford (Hosford (1972)) yield criterion. The von Mises crterion corresponds to a shape parameter $m = 2$,

while the Tresca criterion requires $m \to \infty$.

$$g(\omega) = \sqrt[m]{\left[\cos w - \cos\left(\omega - \frac{2\pi}{3}\right)\right]^m + \left[\cos\left(\omega - \frac{2\pi}{3}\right) - \cos\left(\omega + \frac{2\pi}{3}\right)\right]^m + \left[\cos\left(\omega + \frac{2\pi}{3}\right) - \cos\omega\right]^m} \tag{10}$$

Figure 4 illustrates deviatoric planes for different levels of $\Sigma_m^f = \Sigma_m / |\Sigma_m^{max}|$. Such results were obtained from the macroscopic yield surfaces by the numerically solving Eq. (8) and by considering the modification of the microscopic yield function $\phi(\boldsymbol{\sigma})$ as proposed by Benallal (2017). The $g(\omega)$ function is assumed to follow the Hershey-Dalgreen-Hosford yield criterion as in Eq. (10). Figures 4a and 4b correspond to shape parameter $m = 8$ and $m = 20$, respectively.

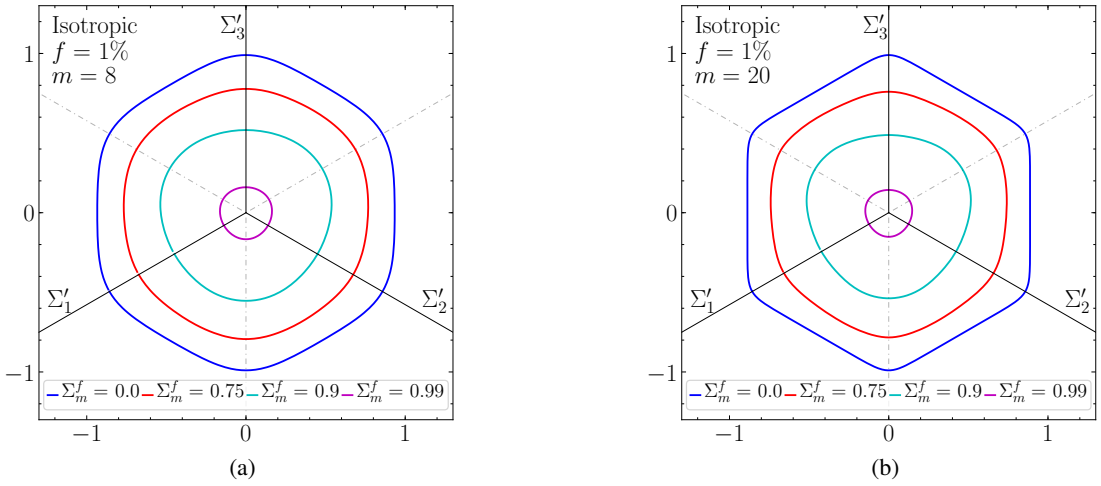

(a) (b)

Figure 4: Benallal (2014) deviatoric planes for different levels of $\Sigma_m^f = \Sigma_m / |\Sigma_m^{max}|$ from macroscopic yield surfaces. The shape parameter (a) $m = 8$ exhibits a transition form between von Mises and Tresca criteria; and (b) $m = 20$ presents sharper edges for $\Sigma_m^f = 0$.

In the same sense as for Fig. 4, Fig. 5 and 6 shows meridional planes macroscopic yield surfaces for $m = 8$ and for $m = 20$, respectively. The mid plane $\theta = \frac{\pi}{6}$ remarkably differs from the axisymmetric ones ($\theta = 0$ and $\theta = \frac{\pi}{3}$), which intensifies here their shifts (to left and right, respectively) with respect to a symmetric plane reference. By generalizing the microscopic yield function, Benallal (2017) constitutive model not only shapes the yield surface on its deviatoric planes, but also increase the influence of the macroscopic Lode angle on its meridional planes.

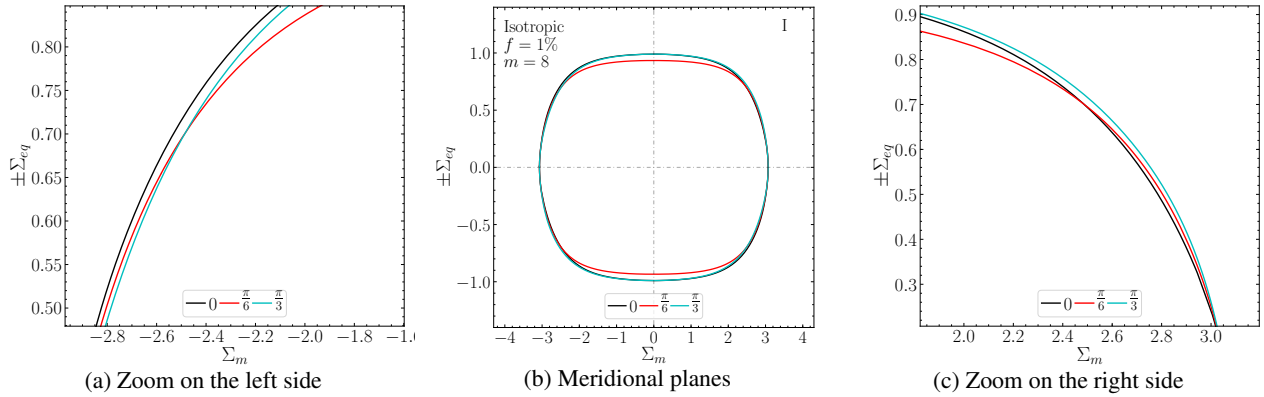

(a) Zoom on the left side (b) Meridional planes (c) Zoom on the right side

Figure 5: Benallal (2014) meridional planes for different macroscopic stress Lode angles θ. The shape parameter is $m = 8$ and the porosity is $f = 1\%$. The microscopic yield stress is assumed to be unitary for simplicity, $\sigma_0 = 1$.

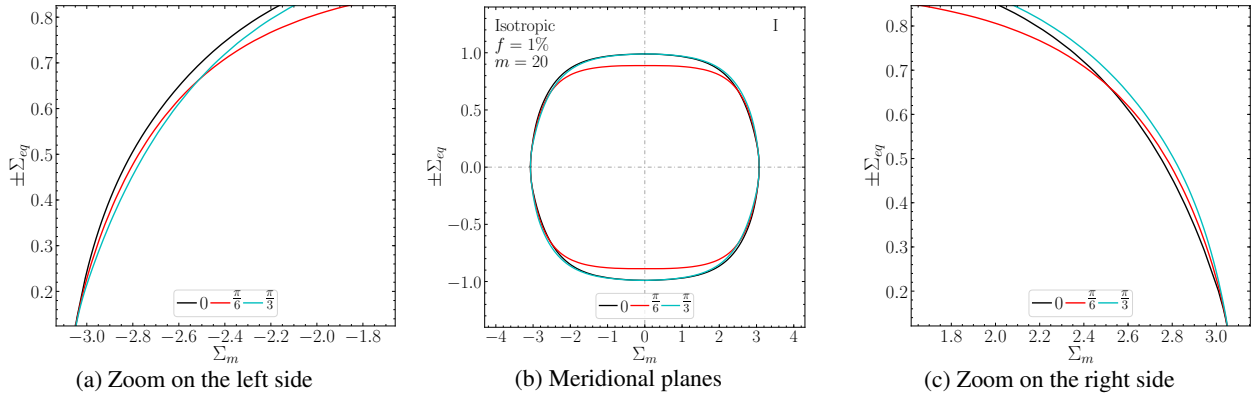

(a) Zoom on the left side (b) Meridional planes (c) Zoom on the right side

Figure 6: Benallal (2014) meridional planes for different macroscopic stress Lode angles θ. The shape parameter is $m = 20$ and the porosity is $f = 1\%$. The microscopic yield stress is assumed to be unitary for simplicity, $\sigma_0 = 1$.

4 GENERALIZED ORTHOTROPIC MATRIX BEHAVIOR WITHIN THE GURSON MODEL APPROACH

Karafilis and Boyce (1993) proposes a procedure based on a linear transformation of a stress tensor $\boldsymbol{\sigma}$ by a 4th order traceless tensor $\mathbb{L}$ so that the resultant fictitious stress tensor $\mathbf{s}$ refer to an Isotropic Plasticity Equivalent (IPE) material, Eq. (11). This procedure allows to define an anisotropic yield function $\psi(\boldsymbol{\sigma})$ by an equivalent manner in terms of an simpler isotropic yield function $\phi(\mathbf{s}ss)$. As the tensor $\mathbb{L}$ performs an affine transformation, the convexity of the isotropic yield function $\phi(\boldsymbol{\sigma})$ is preserved when the argument is the IPE stress tensor $\mathbf{s}$, Eggleston (1969) and Karafilis and Boyce (1993). Throughout this section, the superscript * indicates the analogous variable in IPE space. As $\mathbb{L}$ is traceless, its inverse is only defined in the deviatoric space and indicateddenoted below by the superscript $^+$.

$$\begin{aligned} \mathbf{s} &= \mathbb{L} : \boldsymbol{\sigma} \\ \boldsymbol{\varepsilon}^* &= \mathbb{L}^+ : \boldsymbol{\varepsilon} \end{aligned} \tag{11}$$

In the sense of Gurson (1977) and Benallal (2017), the microscopic yield function $\phi(\boldsymbol{\sigma}) = \sigma_{eq} g(w) - \sigma_0 \leq 0$ can be applied to the IPE stress tensor $\mathbf{s}$ in such way that the convexity of the macroscopic plastic dissipation potential Π, Eq.(12), be preserved (Ferreira, 2018).

$$\Pi(\dot{\mathbf{E}}^*) = \frac{1}{V} \int_V \pi[\dot{\boldsymbol{\varepsilon}}^*_G(\dot{\mathbf{E}}^*)] dV \tag{12}$$

The IPE macroscopic stress tensor and the IPE yield surface are then given by an equivalent way as in the isotropic case, except that now they are defined in the IPE space:

$$\boldsymbol{\Sigma}^* = \frac{\partial \Pi}{\partial \dot{\mathbf{E}}^*} \tag{13}$$

Once the IPE macroscopic yield surface is obtained, the real anisotropic macroscopic yield surface requires that $\boldsymbol{\Sigma}^*$ be transformed back to the anisotropic space stress tensor $\boldsymbol{\Sigma}$ by $\mathbb{L}^+$, Eq. (14). As in the microscopic definition, the preservation of the macroscopic yield surface convexity is guaranteed by the fact that $\mathbb{L}^+$ applies an affine transformation as well as $\mathbb{L}$.

$$\boldsymbol{\Sigma} = \mathbb{L}^+ : \boldsymbol{\Sigma}^* \tag{14}$$

The numerical implementation of this model requires the tensors to be represented as in Voigt notation. In this way, Karafilis and Boyce (1993) show a condensed matrix representation of $\mathbb{L}$ for a material exhibiting a general orthotropic behavior, as in Eq. (15). The components β_1, β_2 and β_3 are obtained by imposing both pressure independence $\mathbb{L}_{ijkk} = 0$ and symmetry $\mathbb{L}_{ijkl} = \mathbb{L}_{klij}$ conditions. Therefore, the tensor $\mathbb{L}$ has 6 independent coefficients, which can be determined experimentally for specific purposes. An additional scalar coefficient C can also be used by multiplying the $\mathbb{L}$ in order adjust its norm. In the following examples, C is chosen so that the norm of the matrix $\mathbf{L}$ in Voigt notation be equal to the

$\sqrt{5}$, which represents the norm of the deviatoric identity $\mathbb{J}$ when written in Voigt notation.

$$\mathbf{L} = C \begin{bmatrix} a & \beta_1 & \beta_2 & 0 & 0 & 0 \\ \beta_1 & b & \beta_3 & 0 & 0 & 0 \\ \beta_2 & \beta_3 & c & 0 & 0 & 0 \\ 0 & 0 & 0 & 2\gamma_1 & 0 & 0 \\ 0 & 0 & 0 & 0 & 2\gamma_2 & 0 \\ 0 & 0 & 0 & 0 & 0 & 2\gamma_3 \end{bmatrix} \tag{15}$$

where $\beta_1 = \frac{c-b-a}{2}$, $\beta_2 = \frac{b-c-a}{2}$ and $\beta_3 = \frac{a-b-c}{2}$.

Figures 7, 8 and 9 contain examples of application of the Gurson model extension hereby presented to orthotropic materials, considering Hershey-Dalgreen-Hosford shape parameters $m = 2$, $m = 8$, $m = 20$, respectively. Both deviatoric planes for different levels of $\Sigma_m^f = \Sigma_m / |\Sigma_m^{max}|$ and meridional ones for different values of microscopic stress Lode angles θ are showed for each macroscopic yield surface obtained. The $\mathbf{L}$ matrix coefficients for the correspondent material symmetries considered in the following analyses are presented in Table 1. In these figures, the orthotropic macroscopic yield surfaces pronounces their preferential directions at deviatoric planes when compared to an isotropic reference. The general edge aspects of the deviatoric planes has been conserved, albeit the orthotropic behavior induces a slight distortion on the shapes. The orthotropic material matrix also intensifies the dependence of meriodional planes on the macroscopic stress Lode angle θ.

Table 1: L transformation coefficients for different material symmetries

Simmetry	a	b	c	f	g	h
Isotropic (I)	1	1	1	0.75	0.75	0.75
Orthotropic (OT)	1	1.25	1.4	1	0.75	0.875

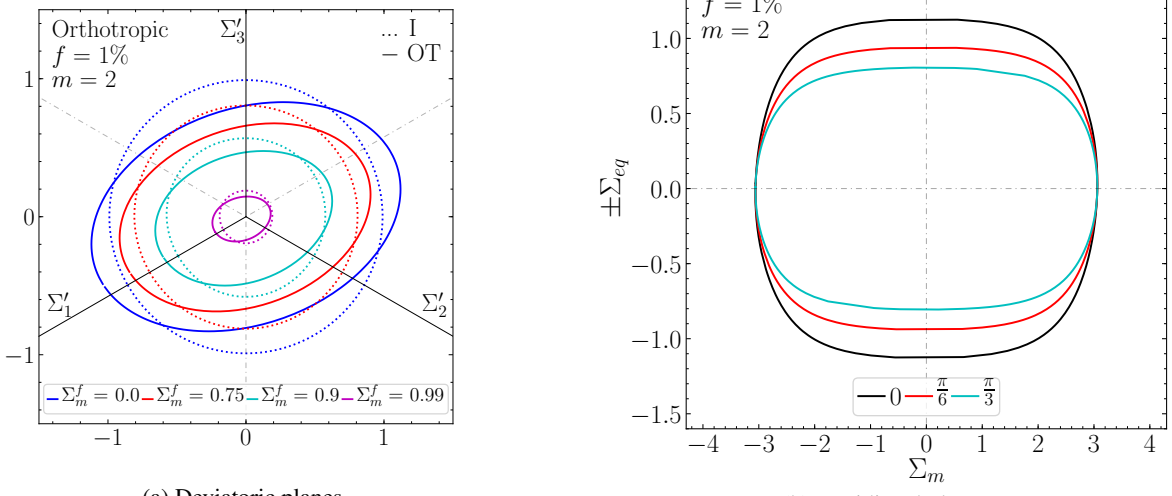

(a) Deviatoric planes

(b) Meridional planes

Figure 7: An orthotropic (OT) macroscopic yield surface obtained for a shape parameter $m = 2$. (a) Deviatoric planes for different levels of $\Sigma_m^f = \Sigma_m / |\Sigma_m^{max}|$ by considering an orthotropic material matrix (OT) and for a isotropic reference (I). (b) Meridional planes for different levels of the macroscopic stress angles θ for an orthotropic material matrix (OT). The microscopic yield stress is assumed to be unitary for sake of simplicity, $\sigma_0 = 1$.

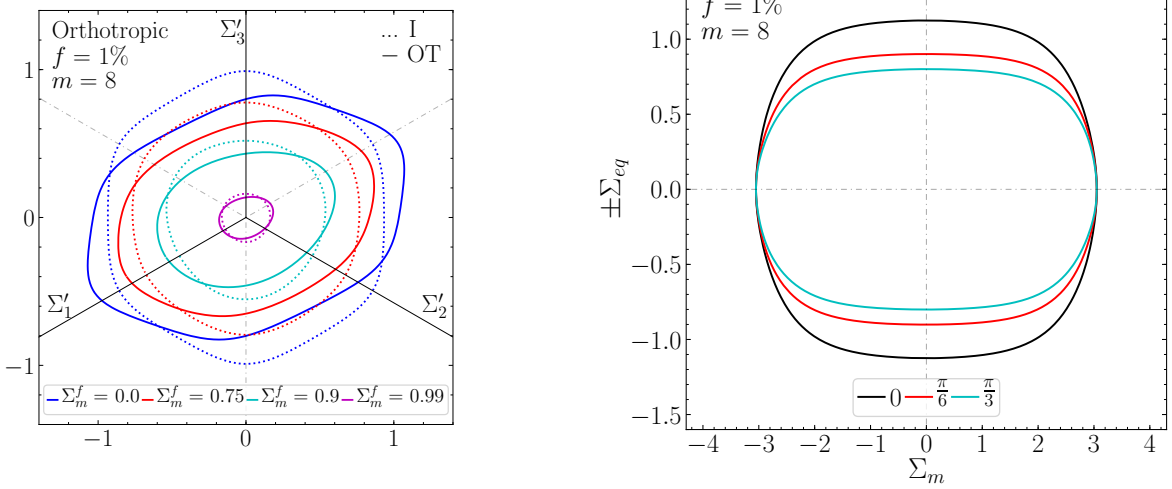

(a) Deviatoric planes

(b) Meridional planes

Figure 8: An orthotropic (OT) macroscopic yield surface obtained for a shape parameter $m = 8$. (a) Deviatoric planes for different levels of $\Sigma^f_m = \Sigma_m/|\Sigma^{max}_m|$ by considering an orthotropic material matrix (OT) and for a isotropic reference (I). (b) Meridional planes for different levels of the macroscopic stress angles θ for an orthotropic material matrix (OT). The microscopic yield stress is assumed to be unitary for sake of simplicity, $\sigma_0 = 1$.

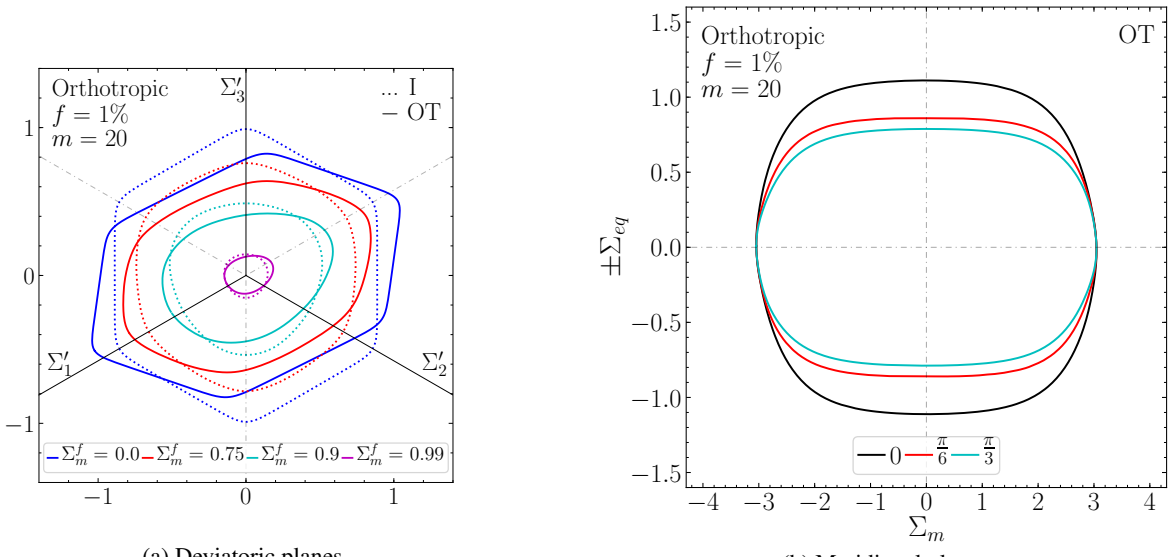

(a) Deviatoric planes

(b) Meridional planes

Figure 9: An orthotropic (OT) macroscopic yield surface obtained for a shape parameter $m = 20$. (a) Deviatoric planes for different levels of $\Sigma^f_m = \Sigma_m/|\Sigma^{max}_m|$ by considering an orthotropic material matrix (OT) and for a isotropic reference (I). (b) Meridional planes for different levels of the macroscopic stress angles θ for an orthotropic material matrix (OT). The microscopic yield stress is assumed to be unitary for sake of simplicity, $\sigma_0 = 1$.

5 CONCLUDING REMARKS

The approach for obtaining orthotropic macroscopic yield surface for ductile rupture processes hereby presented has revealed to be robust, even for high Hershey-Dalgreen-Hosford shape parameters, which implicates in Tresca-like sharp edges to the surface. Moreover, the intensified influence of the macroscopic stress Lode angle on the meridional planes

also consists of an important step in ductile failure modeling, once it tends to generally match several experimental study evidences.

The preferential directions of an orthotropic material have correctly represented situations of ductile rupture, whose severe deformations fields impose crystal dislocations and irreversible elongation of voids and particles. Further work must be devoted to confront this model results with experimental measurements.

6 ACKNOWLEDGMENTS

This study was financed in part by the Coordenação de Aperfeiçoamento de Pessoal de Nível Superior - Brazil (CAPES) - Finance Code 001, by Conselho Nacional de Desenvolvimento Científico e Tecnológico - Brazil (CNPq) and by Centre National de la Recherche Scientifique - France (CNRS).

REFERENCES

Barsoum, I., Faleskog, J., 2011, "Micromechanical analysis on the influence of the Lode parameter on void growth and coalescence", Int. J. Solids Struct., v.48, p.925-38.

Benallal, A., 2017, "Constitutive equations for porous solids with matrix behaviour dependent on the second and third stress invariants", Int. J. Imp. Eng., Vol.108, pp. 47-62.

Benallal, A., Desmorat, R., Fournage, M. 2014, "An assessment of the role of the third stress invariant in the Gurson approach for ductile fracture", J. Euro. Mech. Sol., Vol.47, pp. 400-414.

Broberg, K.B., 1999, "Cracks and Fractures", Cambridge: Academic Press.

Danas, K., Pontes Castañeda, P., 2009. "A finite-sttrain model for anisotropic viscoplastic porous media: I - theory", Euro. J. Mech. A/Solids, Vol.28, pp.685-712.

Egglestone, H.G, 1958, "Convexity", Cambridge University Press.

Ferreira, A.R., 2018. "On the Gurson approach extensions for considering anisotropic constitutive behavior for ductile fracture", PhD thesis, Univeristy of São Paulo/Université Paris-Saclay. (in progress)

Gologanu, M., Leblond, J.-B., Devaux, J., 1993, "Approximate models for ductile metals containing non-spherical voids - case of axisymmetric prolate ellipsoidal cavities" , . Mech. Phys. Solids, Vol.41 No.11, pp.1723-1754.

Gologanu, M., Leblond, J.-B., Devaux, J., 1994. "Approximate models for ductile metals containing non-spherical voids - case of axisymmetric oblate ellipsoidal cavities", J. Eng. Mat. Technol. Vo.116, pp.290-297.

Gurson, A.L., 1977, "Continuum theory of ductile rupture by void nucleation and growth: part I – Yield criteria and flow rules for porous ductile media", J. Eng. Mat. Tech., v.99, p.2-15.

Hosford, W.F., 1972, "A generalized isotropic yield criterion", J Appl Mech, June, pp. 607–609.

Karafilis, A.P., Boyce, M.C., 1993, "A general anisotropic yield criterion using bounds and a transformation weighting tensor", J. Mech. Phys. Solids., Vol.41, No.12, pp. 1859-1886.

Koplik, J., Needleman, A., 1988, "Void growth and coalescence in porous plastic solids", Int. J. Solids Struct., v.24, p.835-53, 1988.

Nahshon, K., Hutchinson, J.W., 2008, "Modification of the Gurson model for shear failure", Eur. J. Mech. V.A27, p.1-17.

Rice, J.R., Tracey, D.M., 1969, "On the ductile enlargement of voids in triaxial stress fields", J. Mech. Phys. Solids., Vol.17, pp. 45-71.

Tvergaard, V., 1981, "Influence of voids on shear band instabilities under plain strain conditions", Int. J. Fract., Vol.17, pp. 389-407.

Tvergaard, V., 1982, "On the localization in ductile materials containing spherical voids", Int. J. Fract., Vol.18, pp. 237-252.

Tvergaard, V., 1990, "Material failure by void growth", Adv. Appl. Mech., Vol.27, pp. 83-151.

Tvergaard, V., Needleman, A., 1984, "Analysis of cup-cone fracture in round tensile bar", Acta. Metallurgica, Vol.32, pp. 157-169.